Aerosol Science and Technology
Publication details, including instructions for authors and subscription information:
http://www.informaworld.com/smpp/title~content=t713656376

Relation between Electrical Mobility, Mass, and Size for Nanodrops 1-6.5 nm in Diameter in Air

Bon Ki Ku [a]; Juan Fernandez de la Mora [b]
[a] Centers for Disease Control and Prevention (CDC), National Institute for Occupational Safety and Health (NIOSH), Cincinnati, Ohio, USA [b] Mechanical Engineering Department, Yale University, New Haven, Connecticut, USA

First Published on: 01 March 2009

To cite this Article Ku, Bon Ki and de la Mora, Juan Fernandez(2009)'Relation between Electrical Mobility, Mass, and Size for Nanodrops 1-6.5 nm in Diameter in Air',Aerosol Science and Technology,43:3,241 — 249
To link to this Article: DOI: 10.1080/02786820802590510
URL: http://dx.doi.org/10.1080/02786820802590510

Aerosol Science and Technology, 43:241–249, 2009

ISSN: 0278-6826 print / 1521-7388 online
DOI: 10.1080/02786820802590510

Relation between Electrical Mobility, Mass, and Size for Nanodrops 1–6.5 nm in Diameter in Air

Bon Ki Ku[1] and Juan Fernandez de la Mora[2]

[1]*Centers for Disease Control and Prevention (CDC), National Institute for Occupational Safety and Health (NIOSH), Cincinnati, Ohio, USA*

[2]*Yale University, Mechanical Engineering Department, New Haven, Connecticut, USA*

A large number of data on mobility and mass have been newly obtained or reanalyzed for clusters of a diversity of materials, with the aim of determining the relation between electrical mobility (Z) and mass diameter $d_m = (6m/\pi\rho)^{1/3}$ (m is the particle mass and ρ the bulk density of the material forming the cluster) for nanoparticles with d_m ranging from 1 nm to 6.5 nm. The clusters were generated by electrospraying solutions of ionic liquids, tetra-alkyl ammonium salts, cyclodextrin, bradykinin, etc., in acetonitrile, ethanol, water, or formamide. Their electrical mobilities Z in air were measured directly by a differential mobility analyzer (DMA) of high resolution. Their masses m were determined either directly via mass spectrometry, or assigned indirectly by first distinguishing singly (z = 1) and doubly (z = 2) charged clusters, and then identifying monomers, dimers, ... n-mers, etc., from their ordering in the mobility spectrum. Provided that $d_m > 1.3$ nm, data of the form d_m vs. $[z(1+m_g/m)^{1/2}/Z)]^{1/2}$ fall in a single curve for nanodrops of ionic liquids (ILs) for which ρ is known (m_g is the mass of the molecules of suspending gas). Using an effective particle diameter $d_p = d_m + d_g$ and a gas molecule diameter $d_g = 0.300$ nm, this curve is also in excellent agreement with the Stokes-Millikan law for spheres. Particles of solid materials fit similarly well the same Stokes-Millikan law when their (unknown) bulk density is assigned appropriately.

INTRODUCTION

Given the fundamental importance of particle size and the ease and precision with which electrical mobility can be measured, a relation between size and mobility reliable down to 1 nm would be of great interest. Such a relation will for brevity be referred generically to as the *mobility law*, or more specifically in the case of spherical particles in air as the *Stokes-Millikan law*. The limitations of existing relations between particle mobility Z and diameter d_p in the nanometer range have been noted in a widely cited article by Tammet (1995). They had been long known in relation to a variety of important problems. For instance, disagreement observed between theoretical and experimental solvated ion size (inferred from mobility) relevant to ion induced nucleation were for a long time attributed to problems in the $Z(d_p)$ relation used, but now appear to have been solved by refinements on the nucleation model (Nadykto et al. 2003). Combined measurements of mobility and mass are often surprisingly informative. For instance, they yield the density of a small spherical cluster, from which one can monitor phase changes (Breaux et al. 2005), provide shape information for non-spherical objects, and even measure the surface energy of single polymer molecules (Ude et al. 2004). Such measurements have been widely used to characterize the shape and structure of biomolecules (Jarrold 2000; Mouradian et al. 1997; Kaufman et al. 1996; Laschober et al. 2007; Kaddis et al. 2007).

The main ambiguities in the $Z(d_p)$ relation for spheres noted by Tammet (1995) involve (i) the need to account for the finite diameter d_g of the bath gas molecules, (ii) the added drag associated to ion dipole interaction (polarization effect), and the expected size dependence of the accommodation coefficient α associated to the fact that gas collisions with large particles tend to be inelastic (α approaching unity and generally taken to be 0.91), while their collisions with small molecular or atomic objects tend to be elastic ($\alpha = 0$). The finite size of the gas molecule can be approximately accounted by simply augmenting the particle diameter d_p in the Stokes-Millikan law (Friedlander 1977) by an effective gas molecule diameter d_g (namely, $d_p = d_m + d_g$):

$$(z/Z) = \left[\frac{3\pi\mu}{e}\frac{(d_m + d_g)}{1 + Kn(1.257 + 0.4\exp^{(-1.1/Kn)})}\right], \quad [1]$$

Received 15 July 2008; accepted 30 October 2008.

We thank Dr. Sven Ude for his valuable comments and contributions to this study. This work was supported by NSF grant CTS-9871885, the National Institute for Occupational Safety and Health grant (Project CAN 9270082), and AFOSR grant FA 9550-06-1-0104.

The mention of any company or product does not constitute an endorsement by the Centers for Disease Control and Prevention. The findings and conclusions in this article are those of the authors and do not necessarily represent the views of the National Institute for Occupational Safety and Health.

Address correspondence to Juan Fernandez de la Mora, Yale University, Mechanical Engineering Department, 9 Hillhouse Ave, New Haven, CT 06520, USA. E-mail: juan.delamora@yale.edu

where Kn is the Knudsen number, defined as $2\lambda/(d_m+d_g)$, λ is the mean free path of the surrounding gas (defined conventionally based on experimental data on the viscosity coefficient μ), and d_m is the mass diameter defined based on the particle mass m and the density ρ of the bulk material of which it is composed

$$m = \frac{\pi}{6}\rho d_m^3 \qquad [2]$$

Several clarifications are required concerning Equation (1). First, any choice of *particle diameter* made in the size range of a few nm is necessarily in some sense arbitrary. Since mass and mobility are the quantities measured here, it is appropriate to define diameters based on both. The mass diameter (Equation [2]) based on bulk density is evidently not a true diameter, since the bulk density does not necessarily apply at nanometer sizes. But d_m has the advantages of being based on well-defined and measurable properties, and of approaching the geometric diameter at relatively small sizes. Second, our choice of the expression given by Friedlander (1977; Equations [2–16], [2–17] and [2–23], with d_p substituted by d_m+d_g) for the *Stokes-Millikan law* is one among several similarly accurate options found in the literature. Kim et al. (2005) give slightly different values for the numerical coefficients in the denominator of Equation (1). Since these two and other alternative expressions collapse into the same free-molecule asymptote, the differences to be expected over the size range covered here (where corrections to the free-molecule limit are tiny) are minimal. For particles below 8 nm we find a maximum discrepancy between Kim et al. and Friedlander of 0.35% in $Z^{1/2}$.

The notion of mobility diameter is less clear-cut than that of mass diameter, and will be used here only as a qualitative guide. If the Stokes-Millikan law $Z = F(d_p)$ did hold strictly, one would define the mobility diameter d_Z associated to a given mobility Z (as often done) through the inverse function $d_Z = F^{-1}(Z)$. If the only modification required to the Stokes-Millikan law were to account for the finite diameter of the gas molecules, then the proper definition of the mobility diameter would be $d_Z = F^{-1}(\mathrm{Z})$ - d_g. And if this shifted mobility diameter coincided with the mass diameter, $d_z = d_m$, then one could write $d_m + d_g = F^{-1}(Z)$, equivalent to the statement $Z = F(d_m + d_g)$ made in Equation (1). This statement, however should not be construed as involving a definition of mobility diameter, nor as an assumption of its identity with the mass diameter. It is merely a hypothesis to be tested. We will simply assemble a variety of data on m and Z, and plot Z vs. $d_g + d_m$ (with d_g treated as a free parameter) in a form permitting extracting simple conclusions regarding the size range of validity of this d_g-shifted Stokes-Millikan law. Notice that the Stokes-Millikan law holds only when the particle mass m is much greater than the mass m_g of the colliding gas molecules. In the free-molecule limit, when $d_p = d_m + d_g \ll \lambda$, the correct form of Equation (1) incorporating the finite particle mass is (Friedlander 1977; Fernandez de la Mora et al. 1998):

$$Z(1+m_g/m)^{-1/2} = \frac{3(2\pi)^{-1/2}}{2(1+\alpha\pi/8)}\frac{q(kT/m_g)^{1/2}}{p(d_m+d_g)^2}, \qquad [3]$$

where k is Boltzmann's constant, T the gas temperature, m_g the mass of the bath gas molecules, q the net charge on the particle ($q = \mathrm{ze}$, where z is charge state and e the elementary charge), and p the pressure. α is the accommodation coefficient measuring the fraction of inelastic collisions characterizing the interaction of the gas molecules with the particle surface. In order for Equation (3) to be consistent with Equation (1) in the limit $d_p \ll \lambda$, α must take the value 0.91, and the particle mass must greatly exceed that of the gas molecules, in which case the numerical coefficient in Equation (3) becomes $3(8\pi)^{-1/2}/(1+\alpha\pi/8) = 0.441$.[1] Although the correction factor $(1+ m_g/m)^{-1/2}$ missing in Equation (1) is generally very close to unity for particles, its elimination carries along errors of several percent for many of our ions (far more for the smallest ones). In order to remove completely this mass dependence of Z, it is convenient to define the effective mobility Z^*:

$$Z^* = Z/(1+m_g/m)^{1/2} \qquad [4]$$

Figure 1a shows our data for the ionic liquid EMI-Im in the form $(6\mathrm{m}/\rho\pi)^{1/3}$ versus $(z/Z^*)^{1/2}$. This peculiar representation has the advantage that both axes are approximately proportional to d_m, so that the Stokes-Millikan law is almost linear in these coordinates. The figure includes mass-corrected $(z/Z^*)^{1/2}$ as well as uncorrected $(z/Z)^{1/2}$ mobility data, showing that the difference is discernible at $d_m = 1.3$ nm. Figure 1a shows both the Stokes-Millikan law (Equation [1]), and its free molecule limit (Equation [3]), displaying a slight difference between the two, in spite of the rather small particle diameters involved ($d_m < 3$ nm). For this reason, we shall subsequently use the full expression (Equation [1]) rather than its simpler limit (Equation [3]). The experimental data shown make use of the masses and mobilities, as well as the measured bulk density of EMI-Im (1515 kg/m^3). The theoretical curve is shifted vertically by the free quantity d_g, assigned here the value $d_g = 0.300$ nm, such that the curve (Equation [1]) goes exactly through the datum with the highest mass. Interestingly, all EMI-Im data fall almost exactly on the reference curve for all mass diameters larger than 1.3 nm. For $d_m < 1.3$ nm the data fall below the theoretical line. This decrease in mobility is qualitatively expected due to polarization effects. In fact, the polarization limit governing point charges gives a constant value of Z^*, corresponding in the case of standard air to a vertical line at $(z/Z^*)^{1/2} \sim 0.71\ (\mathrm{Vs})^{1/2}/\mathrm{cm}$. In the data not including the $(1+ m_g/m)^{1/2}$ correction factor there is a small region at $d_m \sim 1.5$ nm showing a slight increase of Z^* above the Millikan curve. It is tempting to interpret this mobility overshoot as evidence for the reduction in α anticipated by Tammet. But this effect is almost entirely lost once the mass correction is included.

[1] Equation (3) is a hybrid of the kinetic theory result for *elastic hard spheres* ($\alpha = 0$) of arbitrary mass ratios m_g/m, and Epstein's results (Friedlander 1977) for partly *inelastic hard sphere* collisions in the limit $m_g/m \ll 1$. The generalization (Equation [3]) of Epstein's mobility to arbitrary mass ratios follows from the fact that binary interactions are governed by the effective mass $mm_g/(m+m_g)$ rather than either m or m_g.

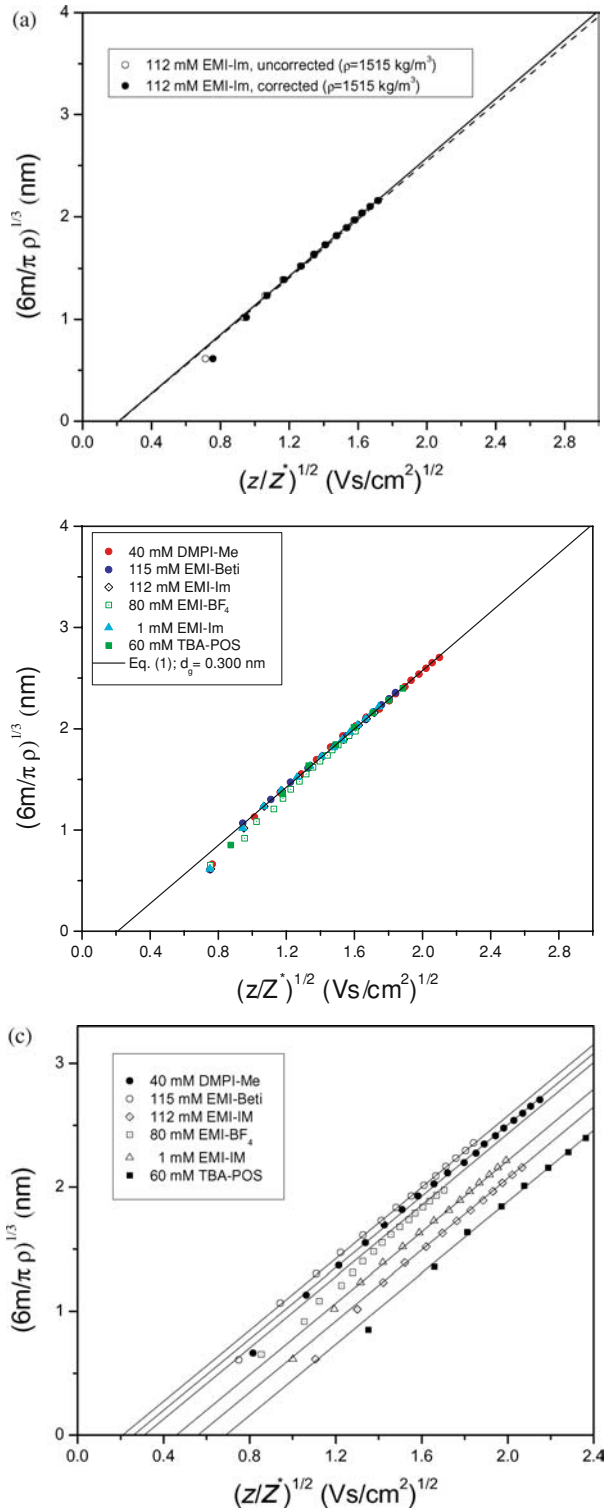

FIG. 1. Compilation of $(6m/\rho\pi)^{1/3}$ versus $(z/Z^*)^{1/2}$ data for clusters of ionic liquids based on their bulk density ρ(except for TBA-POS, whose unknown ρ is chosen such that its data fall right over the curve for EMI-Im). Z^* is the mass-corrected Z (Equation [4]). The continuous line is Equation (1) with an effective gas diameter $d_g = 0.300$ nm. (a) data for EMI-Im. The discontinuous line is the free-molecule limit [3] of Equation (1). (b) Data for all other ionic liquids. (c) data of (b) displaced horizontally for each ionic liquid and the common reference line [1] to display the scatter.

The polarization effect is relatively well understood in the case of elastic collisions between small molecules and atoms (Tammet 1995), but has been studied to a very limited extent for the inelastic situation more typical of nanoparticles (Ude 2004; Gamero-Castaño 1999). The size dependence of the accommodation coefficient has been considered in light of new data by Ude (2004), with some additional discussions contributed by Shandakov et al. (2005), and Li and Wang (2003, 2005, 2006) in part relying on experimental data of Fernandez de la Mora et al. (2003) and Ude et al. (2003, 2004). As noted by Ude (2004), there are still too many unknowns to enable the unambiguous extraction of information on these various mechanisms, whence progress in this field is still strongly dependent on the availability of new data. Most prior studies have used solid nanoparticles with uncertain shapes and densities, including silver (Fernandez de la Mora et al. 2003), polyethylene glycol (PEG) (Ude et al. 2004; Saucy et al. 2004), polystyrene (Ku et al. 2004; Ude et al. 2006), and organic salts (Fernandez de la Mora et al. 2005; Ude and Fernandez de la Mora 2005). Our goal here is to contribute a number of new such data, including some with liquids of known density, more likely to form spherical particles whose mass can be safely converted into a diameter. These nanodrop measurements will then facilitate the interpretation of other solid nanoparticle data.

EXPERIMENTAL

Materials

Table 1 compiles information on the materials (ionic liquids, tetra-alkyl ammonium salts, cyclodextrin, bradykinin, etc.) used in this study as sources of nanoparticles, including their names, abbreviation, concentrations in solution, and molecular weights. The ionic liquids are organic salts with melting points below room temperature. TBA-POS and EMI-BF_4 were from Fluka, and EMI-Im, EMI-Beti, and DMPI-Me from Covalent Associates (Woburn, MA). Tetra-alkyl ammonium salts were from Sigma Chemical Co. and Aldrich Chemical Co., Inc (St. Louis, MO). Acetonitrile was from J. T. Baker (Phillipsburg, NJ), and formamide and ethanol from Sigma Chemical Co. (St. Louis, MO).

Methods

A schematic of the experimental setup is shown in Figure 2 and is similar to that in Ku and Fernandez de la Mora (2004). Briefly, solutions of the different materials in acetonitrile, water, ethanol or formamide (~0.001 up to 1.0 mol/l) were electrosprayed, charge-reduced (to unity) with a 5 mCi Po-210 source (Model P-2042; NRD, Grand Island, NY), and their electrical mobilities were measured using a differential mobility analyzer (DMA) of the Herrmann type. This instrument has unusually high resolution and uses an electrometer as a detector (Eichler 1997; Herrmann et al. 2000). We calibrated the mobility of the clusters using as a standard the known mobility of the dimer ion $A^+(ABr)$ ($1/Z = 1.51$ V s/cm^2), where A^+ stands for the

TABLE 1
Names, concentrations, and molecular weights of various materials used

Material	Name [a]	MW (amu)	Solvent
Ionic liquids	DMPI-Me (40 mM)	550.44	Acetonitrile
	EMI-Beti (115 mM)	491.36	Acetonitrile
	EMI-Im (112 mM)	391.32	Acetonitrile
	EMI-BF_4 (80 mM)	197.98	Acetonitrile
	EMI-Im (1 mM)	391.32	Acetonitrile
	TBA-POS (60 mM)	741.60	Acetonitrile
Organic salts	$(Octyl)_4$N-I (19 mM)	593.77	Ethanol
	$(Dodecyl)_4$N-Br (27 mM)	771.25	Ethanol
	$(Decyl)_4$N-Br (41 mM)	659.0	Ethanol
	$(Hexyl)_4$N-Br (0.971 M)	434.60	Formamide
	THA-Br (5 mM)	490.7	Ethanol
	THA-Br (20 mM)	490.7	Ethanol
	THA-Br (z = 1) [b]	490.7	Formamide
	TBA-TPB (20 mM)	561.7	Acetonitrile
	THA-Br (z = 1) [c]	490.7	Formamide
	TDA-Br (z = 1) [d]	659.0	Propanol
Peptide	Bradykinin (17.9 mM)	1060.2	Water
Cyclic sugar	Cyclodextrin (10 mM)	1135.0	Water
Polymer	PEG (z = 1) [e]	440–1080	Water/Methanol
	PEG (z = 2) [e]	1080–3000	Water/Methanol
	Polystyrene [f]	9200	NMP [g]

[a]Material names are abbreviated for simplicity. [b]Gamero and Fernandez de la Mora (2000); [c]Fernandez de la Mora et al. (2005); [d]Ude and Fernandez de la Mora (2005); [e]Ude et al. (2004); [f]Ude et al. (2006); [g]NMP = 1-methyl-2-pyrrolidone

DMPI: 1,2-dimethyl-3-propylimidazolium.
EMI: 1-ethyl-3-methylimidazolium = $(C_6H_{11}N_2)^+$.
Beti: bis(perfluoroethylsulfonyl)imide.
Im: bis(trifluoromethylsulfonyl)imide = $N(SO_2CF_3)_2^-$.
BF_4: tetrafluoroborate.
Me: tris(trifluoromethylsulfonyl)methide = $C(SO_2CF_3)_3^-$.
TBA: Tetrabutylammonium.
POS: perfluorooctanesulfonate.
TPB: tetraphenylborate.
PEG: Poly(ethylene glycol).
THA: Tetraheptyl ammonium.
TDA: Tetradecyl ammonium.

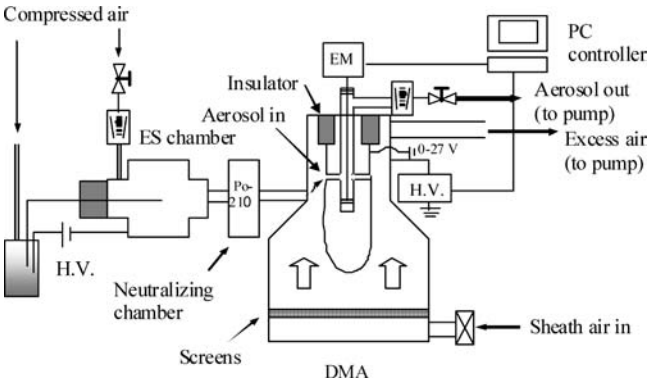

FIG. 2. Experimental setup. EM = Electrometer; ES = Electrospray; H.V. = High Voltage Power Supply; DMA = Differential Mobility Analyzer.

tetraheptylammonium cation (Gamero-Castaño and Fernández de la Mora 2000). The standard tetraheptylammonium$^+$ ion is electrosprayed from a dilute (∼1 mM) alcohol solution. The measurements were taken under laboratory conditions of pressure (sea level) and temperature, without recording their precise values. Pressure corrections are taken exactly into account through the use of the tetraheptylammonium standard. Temperature variations are only approximately corrected in this normalization (as is generally the case in ion mobility measurements referred to standard conditions of temperature). However, uncorrected temperature variations of our mobilities are very small due to (i) the small range of variation of the laboratory temperature and (ii) the small differences in the temperature dependence of the mobilities of these cluster ions and the tetraheptylammonium$^+$ standard used. An upper limit can be given since our largest ions behave approximately as hard spheres, for which $Z \sim T^{1/2}$, while $Z \sim T$ for point charges in the polarization limit. Assuming a variation of T as large as 5°C above or below the temperature at which the standard was measured, the maximum uncorrected error in Z would be 0.8%. In reality the ion standard used has a mobility 3 times smaller than the polarization limit, and is probably closer to the hard sphere behavior with an uncorrected temperature dependence most likely smaller than $T^{1/4}$ (expected maximum error below 0.4%). Note for reference that errors associated to variations in the sheath gas velocity (taking place between the cluster and the standard mobility measurements) are estimated to be larger than 1%. The greatest ambiguity in our mobility measurements is associated to the mobility standard used, but this problem can be simply repaired in the future, once a better value is obtained for this standard. Another ambiguity is due to the fact that the drift gas was filtered room air at its ambient (unmeasured) humidity level.

With only some exceptions to be noted, particle mass was not directly measured by a mass spectrometer, but was established indirectly by first distinguishing singly and doubly charged clusters, and then determining the number n in the structure $(AB)_nA^+$ of the singly charged series of ions based on the ordering (n = 0, 1, 2, etc.) of the corresponding mobility peaks observed. More details on the procedure are given by Ku and Fernandez de la Mora (2004).

RESULTS

Mobility Measurement and Mass Assignments of Clusters

Figure 3 shows typical mobility spectra for DMPI-Me, including peak assignments. Figure 3a represent a mobility spectrum as electrosprayed, and Figure 3b is a mobility spectrum after charge reduction. Both figures are adapted from Figure 2 of Ku and Fernandez de la Mora (2004). One sees first a discrete region to the left in Figure 3a, where individual peaks rise in isolation. Then follows a fairly crowded region between about 1.5 and 3 Vs/cm^2, where a denser group of peaks rises above what appears as a continuous background. All the mobility spectra for the other materials used are similar to those for DMPI-Me.

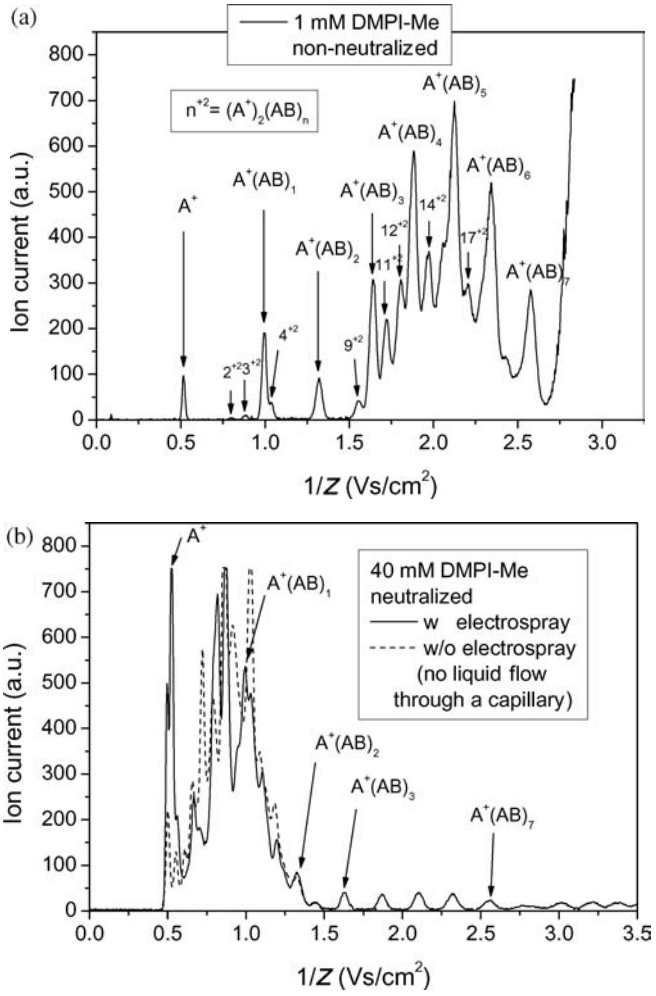

FIG. 3. Mobility spectra of DMPI-Me, where A and B denote $C_8H_{15}N_2^+$ and $C(SO_2CF_3)_3^-$, respectively: (a) naturally charged electrosprays. (b) charge-reduced electrosprays enabling identification on singly charged ions. The dashed line is taken without electrospray and contains only ions from the polonium source. Adapted from FIG. 2 of Ku and Fernandez de la Mora (2004).

The apparently continuous background is in reality the superposition of numerous isolated peaks associated with relatively large multiply charged clusters. Their mobilities tend to lie in a restricted range because these clusters are formed as charged residues from dry electrospray drops evolving in the ion evaporation regime (Loscertales and Fernandez de la Mora 1995). Positively charged clusters generated by electrosprays have the form $(AB)_nA_z^+$, where z is the charge state and n the state of aggregation. Singly charged ions were identified independently by comparing naturally charged (without a neutralizer) and charge-reduced ($z = 1$ with a neutralizer) mobility spectra, because, after charge reduction, singly charged ions remain in their original positions in the spectrum, whereas multiply charged ions shift to lower mobilities, as shown in Figure 3b. Earlier work based on a detector sensitive to the charge state (Gamero-Castaño and Fernandez de la Mora 2000) or on a mass spectrometer (Fernandez de la Mora et al. 2005) has shown that the discrete region in Figure 3a contains only singly and doubly charged clusters ($z = 1, 2$), whereas charge states larger than 2 lie in the region of the continuous background. For this reason, ions in the discrete region known not to be singly charged in Figure 3a are provisionally presumed to correspond to $z = 2$. New mass versus mobility data for the different materials are collected in Table 2.

Figure 1b shows data for all the other ionic liquids (ILs) studied. We have used published bulk densities for all except for TBA-POS, for which ρ is only available well above room temperature [$\rho = 1313\,\text{kg/m}^3$ at 121°C; Pomaville and Poole (1989, 1990)]. The data for TBA-POS are plotted based on the density $\rho = 1250\,\text{kg/m}^3$, chosen such that the datum for the largest mass available fall right on top of the curve for EMI-Im (see Table 3). The solid line is from Equation (1) with $d_g = 0.300$ nm. Excepting the data for the monomers and dimers, and excepting also those for EMI-BF_4, all the points fall closely on the same curve previously defined by EMI-Im. The scatter in the monomer data is to be expected, since all have essentially the same mobility (polarization limit) but correspond to different masses and densities. Note that many of the data points correspond to the common EMI^+ ion, and still exhibit some scatter due to the assumption of a density equal to the bulk density, independently of size. Given the different densities of the anions and cations, this assumption is evidently inappropriate for salt clusters with moderate n values (having $n+1$ cations and n anions). It would have in fact made more sense to use cluster volume instead of m/ρ for the vertical variable of this figure, but this refinement is unwarranted given the importance of polarization and other ignored effects at such small sizes. The anomalous behavior of EMI-BF_4 is difficult to ascertain. Given the small size of the BF_4 anion, the clustering level n is considerably larger for EMI-BF_4 nanodrops than for other IL clusters of similar mass, suggesting that our assignment of n may be incorrect. This liquid should therefore be reexamined combining mobility and direct mass measurements. Except for the anomalies noted, the data appear to collapse quite closely in Figure 1b. However, there is some clear scatter, which can be better appreciated by comparing separately the data for each ionic liquid with a common reference. This is done in Figure 1c by displacing horizontally each of the data sets in Figure 1b, together with the theoretical line for $d_g = 0.300$ nm. The final figure shows among other things a slight but clear vertical displacement for EMI-Beti, suggesting a density a little larger than the published value.

We conclude from this initial study with ionic liquid clusters that the conventional $Z(d_p)$ relation with $d_p = d_m + 0.300$ nm is surprisingly accurate down to $d_m = 1.3$ nm. We also find that bulk density data may be used reliably to infer the mass diameter, at least with nanodrops. This second observation is of great practical interest in nanoparticle studies, particularly given the vast number of ionic liquids already available, and their notable property of being essentially involatile.

We have also examined a number of materials whose bulk form at room temperature is solid. A first subgroup among these

TABLE 2a
Mass and inverse mobility of the singly charged ions observed for various materials. Z is pressure and temperature corrected by normalization with a mobility standard

Ion	Mass (amu)	$1/Z$ [a]	Mass (amu)	$1/Z$ [a]	Mass (amu)	$1/Z$ [a]	Mass (amu)	$1/Z$ [a]	Mass (amu)	$1/Z$ [a]
z = 1	$(Hexyl)_4N$-Br		$(Dodecyl)_4N$-Br		Bradykinin		Cyclodextrin		TBA-TPB	
A^+	354.7	0.94	691.29	1.397	1060.2	1.41	1135	1.49	242.5	0.72
$A^+(AB)$	789.3	1.42	1462.5	2.016	2120.4	2.09	2270	2.02	804.2	1.37
$A^+(AB)_2$	1223.9	1.74	2233.8	2.593	3180.6	2.66	3405	2.58	1365.9	1.66
$A^+(AB)_3$	1658.5	2.02	3005.0	3.083	4240.8	3.18	4540	3.04	1927.6	2
$A^+(AB)_4$	2093.1	2.27	3776.3	3.454	5301	3.64	5675	3.5	2489.3	2.22
$A^+(AB)_5$	2527.7	2.57	4547.5	3.867	6361.2	4.1	6810	3.9	3051.0	2.42
$A^+(AB)_6$	2962.3	2.89	5318.8	4.269	7421.4	4.49	7945	4.37	3612.6	2.59
$A^+(AB)_7$	3396.9	3.14	6090.0	4.646	8481.6	4.9			4174.4	2.79
$A^+(AB)_8$	3831.5	3.39	6861.3	4.976	9541.8	5.31			4736.1	2.94
$A^+(AB)_9$	4266.1	3.65	7632.5	5.321	10602	5.66			5297.8	3.13
$A^+(AB)_{10}$	4700.7	3.89	8403.8	5.646	11662	6.01			5859.7	3.36
$A^+(AB)_{11}$			9175.0	6.023					6421.2	3.61
$A^+(AB)_{12}$			9946.3	6.307					6982.9	3.9
$A^+(AB)_{13}$			10717	6.539					7544.6	4.11
$A^+(AB)_{14}$									8106.3	4.41

[a] Vs/cm^2.

has been previously investigated with simultaneous determination of mobility and mass (with a mass spectrometer). These more completely characterized clusters include PEG (Ude et al. 2004), polystyrene (Ude et al. 2006), TDA-Br (Ude et al. 2005), and THA-Br (Fernandez de la Mora et al. 2005). Figure 4a shows the corresponding data in the form $(6m/\rho\pi)^{1/3}$ versus $(z/Z^*)^{1/2}$ together with the reference curve (1) with $d_g = 0.300$ nm. The bulk densities of these materials are unknown. The densities used to construct the figure are listed in Table 3, as determined with the criterion that the datum with the maximum possible mass

TABLE 2b
Mass and inverse mobility of the singly charged ions observed for ionic liquids. Z is pressure and temperature corrected by normalization with a mobility standard

Ion	Mass (amu)	$1/Z$ [a]	Mass (amu)	$1/Z$ [a]	Mass (amu)	$1/Z$ [a]	Mass (amu)	$1/Z$ [a]	Mass (amu)	$1/Z$ [a]	Mass (amu)	$1/Z$ [a]
z = 1	DMPI-Me		EMI-Beti		EMI-Im (112 mM)		$EMI-BF_4$		EMI-Im (1mM)		TBA-POS	
A^+	139.22	0.534	111.168	0.502	111.168	0.509	111.168	0.507	111.168	0.503	242.46	0.72
$A^+(AB)$	689.66	1.007	602.528	0.869	502.488	0.879	309.148	0.870	502.488	0.867	984.06	1.37
$A^+(AB)_2$	1240.1	1.339	1093.888	1.218	893.808	1.128	507.128	1.022	893.808	1.119	1725.66	1.76
$A^+(AB)_3$	1790.54	1.649	1585.248	1.485	1285.128	1.359	705.108	1.245	1285.128	1.353	2467.26	2.21
$A^+(AB)_4$	2340.98	1.884	2076.608	1.748	1676.448	1.601	903.088	1.371	1676.448	1.580	3208.86	2.54
$A^+(AB)_5$	2891.42	2.119	2567.968	1.983	2067.768	1.802	1101.068	1.483	2067.768	1.781	3950.46	2.91
$A^+(AB)_6$	3441.86	2.340	3059.328	2.186	2459.088	1.985	1299.048	1.612	2459.088	1.969	4692.06	3.24
$A^+(AB)_7$	3992.3	2.578	3550.688	2.397	2850.408	2.172	1497.028	1.717	2850.408	2.170	5433.66	3.54
$A^+(AB)_8$	4542.74	2.781	4042.048	2.585	3241.728	2.348	1695.008	1.825	3241.728	2.325		
$A^+(AB)_9$	5093.18	3.041	4533.408	2.767	3633.048	2.491	1892.988	1.940	3633.048	2.465		
$A^+(AB)_{10}$	5643.62	3.245	5024.768	2.924	4024.368	2.630	2090.968	2.062	4024.368	2.609		
$A^+(AB)_{11}$	6194.06	3.380	5516.128	3.084	4415.688	2.784	2288.948	2.145	4415.688	2.768		
$A^+(AB)_{12}$	6744.5	3.583	6007.488	3.248	4807.008	2.938	2486.928	2.253	4807.008	2.897		
$A^+(AB)_{13}$	7294.94	3.729	6498.848	3.380			2684.908	2.350	5198.328	3.031		
$A^+(AB)_{14}$	7845.38	3.911					2882.888	2.447				
$A^+(AB)_{15}$	8395.82	4.071										
$A^+(AB)_{16}$	8946.26	4.224										
$A^+(AB)_{17}$	9496.7	4.406										

[a] Vs/cm^2.

TABLE 3
Bulk and assigned particle densities ρ for different materials

Material	Bulk ρ^a (kg/m^3)	Calculated ρ^c (kg/m^3)
DMPI-Me (40 mM)	1520	
EMI-Beti (115 mM)	1570	
EMI-Im (112 mM)	1515	
EMI-BF_4 (80 mM)	1267	
EMI-Im (1mM)	1515	
TBA-POS (60 mM)	1313^b	1250
$(Octyl)_4$N-I (19 mM)		926
$(Dodecyl)_4$N-Br (27 mM)		879
$(Decyl)_4$N-Br (41 mM)		875
TBA-TPB (20 mM)		1275
Bradykinin (17.9 mM)		1098
Cyclodextrin (10 mM)		1269
$(Hexyl)_4$N-Br (0.971M)		911
THA-Br (5 mM)		892
THA-Br (20 mM)		903
THA-Br (5.35 mM)		892
(Gamero and de la Mora 2000)		
PEG ($z = 1$) (Ude et al. 2004)		1099
PEG ($z = 2$) (Ude et al. 2004)		1095
Polystyrene (Ude et al. 2006)		942
THA-Br ($z = 1$) (de la Mora et al. 2005)		947
TDA-Br ($z = 1$) (Ude et al. 2005)		861

[a] Bulk densities of most ionic liquids were measured at room temperatures, except DMPI-Me and EMI-Beti, for which they were obtained from the manufacturer (www.strem.com).

[b] Measured at 121°C by Pomaville and Poole (1989, 1990).

[c] Obtained by forcing the datum with the highest mass within the range of EMI-Im data to go through the curve for EMI-Im.

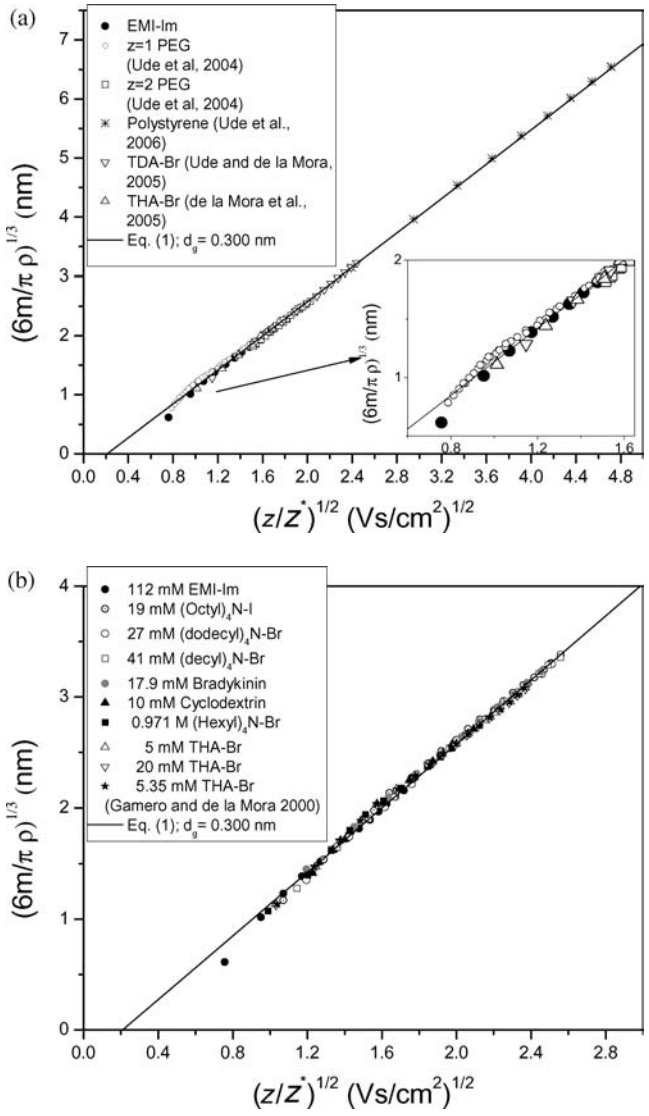

FIG. 4. Compilation of $(6m/\rho\pi)^{1/3}$ versus $(z/Z^*)^{1/2}$ data for various solid materials for which the unknown bulk density ρ is determined so as to match the curve for EMI-Im. The continuous line is Equation (1) with $d_g = 0.300$ nm. (a) data for PEG, polystyrene, TDA-Br, and THA-Br, for which data for both m and Z exist. For PEG with $z = 2$, only the data for which Ude et al. (2005) report spherical shapes are included. The concentration of the EMI-Im is 112 mM. (b) Data for the indicated substances for which m is determined indirectly.

falls right on the curve for EMI-Im. With the exception of PEG all the data fall on a single curve, which coincides with Equation (1) in the size range 1.3 nm $< d_m <$ 6 nm. The exception of the open circles associated to PEG is noteworthy, as its magnitude clearly exceeds the small scatter seen in the other materials. Because these data involved direct mass determination, they reveal a true increase in mobility at $d_m \sim$1.5 nm. Ude (2004) had previously noted this anomaly, and interpreted it in light of Tammet's ideas as due to a decrease in the accommodation coefficient α. But this explanation loses force in view of the fact that it does not apply to any of the other clusters investigated. A more likely explanation is that PEG undergoes a transformation below 1.5 nm, either by densification or by adoption of a more compact structure. Although melting could take place below a certain critical size, it would tend to increase rather than reduce density. It is therefore unclear what the observed restructuring could be.

Figure 4b includes data for all the other solid materials of unknown bulk density studied, whose mass is determined indirectly from the sequence of mobility peaks. The theoretical curve shown is from Equation (1) with $d_g = 0.300$ nm. The best-fit densities used to define the vertical coordinate are determined as before. The proximity of the data to Equation (1) is comparable to that shown previously, except for the TBA-TPB clusters (not shown in Figure 4b). Similarly as in the case of EMI-BF_4, this series should be reexamined by combined mobility and mass spectrometry measurements. Several of the data sets falling close to the theoretical line exhibit a small region slightly above the Stokes-Millikan line.

As an additional test, our data for THA-Br were compared with those of Fernandez de la Mora et al. (2005), for which

both mass and mobility were directly measured, and where a particle density of 935 kg/m^3 was inferred from all the clusters investigated, including multiply charged ones. In the present study, we have studied singly charged THA-Br clusters at two different concentrations (5 mM and 20 mM). The particle densities inferred by adjusting the datum with the highest mass to go through the standard curve of the EMI-Im are 892 kg/m^3 and 903 kg/m^3, respectively, as shown in Table 3. The disagreements with the density of Fernandez de la Mora et al. are 4.6% and 3.4%, respectively. This difference may be due to the less accurate calibration of the mobility scale in the previous study, carried out in a brief visit to the Sciex laboratory, meant more to provide a qualitative demonstration of the power of the DMA-MS combination than to achieve an accurate measurement of nanoparticle density. Fernandez de la Mora et al. (2005) have noted a decrease in the mobility of the multiply charged THA-Br with respect to the singly charged ones. Their figures did not make the $(1+m_g/m)^{1/2}$ mobility correction used here, but the difference remains even after including it. This points to the need to include polarization effects for the doubly as well as the singly charged particles.

Some indication of the potential of tandem measurements of mobility and mass to infer nanoparticle density can be seen in Figure 5, which replots the same data previously represented in terms of mass diameter based on an artificial density of 1000 kg/m^3. The data spread into a wide fan rather than a single curve, since the densities span a wide range from 861 to 1513 kg/m^3. Note that any mass versus mobility data set could be plotted in this format even in the absence of density information. The reference theoretical lines included (based on Equation [1] with $d_g = 0.300$ nm) evidently require density information. They are included to provide a direct graphical density scale from which the unknown density of the nanoparticles in a (Z, m) data set could be inferred fairly reliably. In this fan we have used the data for EMI-Im with its bulk density and the free parameter d_g to achieve an optimal fit. The density inferred in this fan representation based on the (Z, m) data for the other materials would then not necessarily agree with their bulk densities. But they do agree well, as evident from the fact that all the data collapse closely in the representation of Figures 1 and 4. For instance, the density determined in this way for DMPI-Me is 1513 kg/m^3, very close to the bulk density of 1520 kg/m^3. This good agreement is encouraging given that a growing literature using the GEMMA system (Kaufman et al. 1996) commercialized by TSI, consistently concludes that achieving a good fit between measured protein mobilities and known protein masses requires the assumption that the protein density is approximately half of its bulk value (Kaddis et al. 2007; Laschober et al. 2007). Note finally that the density determination scheme just discussed is only applicable to spherical nanoparticles. For nonspherical particles of known density, the same procedure would yield valuable shape information.

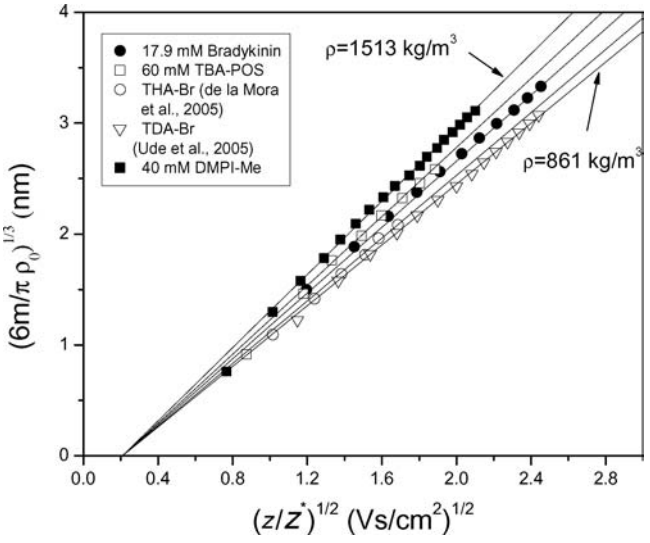

FIG. 5. $(6m/\rho_0\pi)^{1/3}$ versus $(z/Z^*)^{1/2}$ curves ($\rho_0 = 1000$ kg/m^3), similar to Figures 1 and 4, but with the vertical variable rescaled by the ratio $(\rho/\rho_0)^{1/3}$, to illustrate how a set of Z(m) data could be used to infer material density ρ. The data cover the full density range available, from 861 kg/m^3 to 1513 kg/m^3. The densities corresponding to the lines shown are 861, 947, 1098, 1250, and 1513 kg/m^3, respectively, starting on the lower line.

CONCLUSIONS

1. Measurements with nanodrops of ionic liquids (ILs) validate accepted $Z(d_p)$ expressions down to $d_m = 1.3$ nm, provided that one uses as effective drop diameter $d_p = d_m + 0.300$ nm. This observation confirms also the notion that the densities of these nanodrops are close to bulk values.
2. Based on a best fit *cluster density*, a similarly good agreement is found for other solid materials tested for which bulk densities are unavailable.
3. These results demonstrate that the established relation between electrical mobility and mass diameter for a sphere can be applied with confidence over the whole size range down to $d_m = 1.3$ nm.
4. One should note as exceptions to the prior conclusions that the data for the ionic liquid EMI-BF_4 and the solid salt TBA-TBP depart considerably from the established Stokes-Millikan law. The general applicability of our conclusions on the Stokes-Millikan law should therefore not be taken for granted until these two anomalous materials (out of a total of 19 studied) are reexamined with direct mass measurement. An additional limitation of this work is the lack of corrections associated to polarization. This correction could be carried out approximately based on the findings of Ude (2004), but will be delayed until Ude's correction is better established.
5. Notwithstanding the widely reported anomalous density of proteins inferred from their theoretical mass and their mobility measured by GEMMA, we find nanoparticle densities in excellent agreement with bulk values.

REFERENCES

Breaux, G. A., Cao, B. P., and Jarrold, M. F. (2005). Second-Order Phase Transitions in Amorphous Gallium Clusters, *J. Chem. Phys. B*, 109(35):16575–16578.

Eichler, T. A. (1997). Differential Mobility Analyzer for Ions and Nanoparticles: Laminar Flow at High Reynolds Numbers, Senior Graduation Thesis, Fachhochschule Offenburg, Germany.

Fernandez de la Mora, J., de Juan, L., Eichler, T., and Rosell, J. (1998). Differential Mobility Analysis of Molecular Ions and Nanometer Particles, *Trends in Analytical Chemistry,* 17:328–339.

Fernandez de la Mora, J., de Juan, L., Liedtke, K., and Schmidt-Ott, A. (2003). Mass and Size Determination of Nanometer Particles by Means of Mobility Analysis and Focused Impaction, *J. Aerosol Sci*., 34:79–98.

Fernandez de la Mora, J., Thomson, B., and Gamero-Castaño, M. (2005). Tandem Mobility Mass Spectrometry Study of Electrosprayed $Heptyl_4N^+Br^-$ Clusters, *J. Am. Soc. Mass Spectrom*., 16:717–732.

Friedlander, S. K. (1977). *Smoke, Dust, and Haze*. Wiley, New York, pp. 6, 31.

Gamero-Castaño, M. (1999). The Transfer of Ions and Charged Nanoparticles from Solution to the Gas Phase in Electrosprays, Ph.D. Thesis, Yale University, Mechanical Engineering Department.

Gamero-Castaño, M., and Fernandez de la Mora, J. (2000). Mechanisms of Electrospray Ionization of Singly and Multiply Charged Salt Clusters, *Anal. Chim. Acta*., 406, 67.

Herrmann, W., Eichler, T., Bernardo, N., and Fernandez de la Mora, J. (2000). Turbulent Transition Arises at Reynolds Number 35,000 in a Short Vienna Type DMA with a Large Laminarization Inlet, *Abstract to the Annual Conference of the AAAR*, St Louis, Missouri.

Jarrold, M. F. (2000). Peptides and Proteins in the Vapor Phase, *Ann. Rev. Phys. Chem*., 51:179–207.

Kaddis, C. S., Lomeli, S. H., Yin, S., Berhane, B., Apostol, M. I., Kickhoefer, V. A., Rome, L. H., and Loo, J. A. (2007). Sizing Large Proteins and Protein Complexes by Electrospray Ionization Mass Spectrometry and Ion Mobility, *J. Am. Soc. Mass Spectr*., 18(7):1206–1216.

Kaufman, S. L., Skogen, J. W., Dorman, F. D., Zarrin, F., and Lewis, L. C. (1996). Macromolecule Analysis Based on Electrophoretic Mobility in Air: Globular Proteins, *Anal. Chem*., 68:1895–1904.

Kim, J. H., Mulholland, G. W., Kukuck, S. C., and Pui, D. Y. H. (2005). Slip Correction Measurements of Certified PSL Nanoparticles Using a Nanometer Differential Mobility Analyzer (Nano-DMA) for Knudsen Number from 0.5 to 83, *J. Res. Natl. Inst. Stand. Technol.* 110:31–54.

Ku, B. K., and Fernandez de la Mora, J. (2004). Cluster Ion Formation in Electrosprays of Acetonitrile Seeded with Ionic Liquids, *J. Phys. Chem. B*, 108(39):14915–14923.

Ku, B. K., Fernandez de la Mora, J., Saucy, D. A., and Alexander, J. N. (2004). Mass Distribution Measurement of Water-Insoluble Polymers by Charge-Reduced Electrospray Mobility Analysis, *Anal. Chem*. 76:814–822.

Laschober, C., Kaddis, C. S., Reischl, G. P., Loo, J. A., Allmaier, G., and Szymanski, W. W. (2007). Comparison of Various Nano-Differential Mobility Analysers (nDMAs) Applying Globular Proteins, *J. Exper. Nanosci*. 2(4):291–301.

Li, Z. G., and Wang, H. (2003). Drag Force, Diffusion Coefficient, and Electric Mobility of Small Particles. I. Theory Applicable to the Free-Molecule Regime, *Phys. Rev. E*, 68(6):Article Number: 061206.

Li, Z. G., and Wang, H. (2005). Gas-Nanoparticle Scattering: A Molecular View of Momentum Accommodation Function, *Phys. Rev. Lett*., 95(1): Article Number: 014502.

Li, Z. G., and Wang, H. (2006). Comment on "Phenomenological Description of Mobility of nm- and sub-nm-Sized Charged Aerosol Particles in Electric Field" by Shandakov, S. D., Nasibulin, A. G. and Kauppinen, E. I., *J. Aerosol Sci*., 37(1):111–114.

Loscertales, I. G., and Fernandez de la Mora, J. (1995). Experiments on the Kinetics of Field Evaporation of Small Ions from Droplets, *J. Chem. Phys*., 103:5041.

Mouradian, S., Skogen, J. W., Dorman, F. D., Zarrin, F, Kaufman, S. L., and Smith, L. M. (1997). DNA Analysis Using an Electrospray Scanning Mobility Particle Sizer, *Anal. Chem*. 69:919–925.

Nadykto, A. B., Makela, J. M., Yu, F. Q., Kulmala, M., and Laaksonen A. (2003). Comparison of the Experimental Mobility Equivalent Diameter for Small Cluster Ions with Theoretical Particle Diameter Corrected by Effect of Vapour Polarity, *Chem. Phys. Lett*., 382(1–2):6–11.

Pomaville, R. M., and Poole, C. F. (1989). Changes in Retention and Polarity Accompanying the Replacement of Hydrogen by Fluorine in Tetraalkylammonium Alkyl- and Arylsulfonate Salts used as Stationary Phases in Gas Chromatography, *J. Chromatography A,* 468:261–278.

Pomaville, R. M., and Poole, C. F. (1990). Gas Chromatographic Study of the Solution Thermodynamics of Organic Solutes in Tetraalkylammonium Alkanesulfonate and Perfluoroalkanesulfonate Solvents, *J. Chromatography,* 499:749–759.

Saucy, D., Ude, S., Lenggoro, W., and Fernandez de la Mora, J. (2004). Mass Analysis of Water-Soluble Polymers by Mobility Measurement of Charge-Reduced Electrosprays, *Anal. Chem*. 76:1045

Shandakov, S. D., Nasibulin, A. G., and Kauppinen, E. I. (2005). Phenomenological Description of Mobility of nm- and sub-nm-Sized Charged Aerosol Particles in Electric Field, *J. Aerosol Sci*. 36(9):1125–1143.

Tammet, H. (1995). Size and Mobility of Nanoparticles, Clusters and Ions, *J. Aerosol Sci*. 26:459–475.

Ude, S. (2004). Measurement and Properties of Nanometer Particles in the Gas Phase, Ph.D. Thesis, Yale University, Chemical Engineering Department.

Ude, S., and Fernandez de la Mora, J. (2005). Molecular Monodisperse Mobility and Mass Standards from Electrosprays of Tetra-Alkyl Ammonium Halides, *J. Aerosol Sci*. 36:1224–1237.

Ude, S., Fernandez de la Mora, J., and Thomson, B. A. (2004). Charge-Induced Unfolding of Multiply Charged Polyethylene Glycol Ions, *J. Am. Chem. Soc*. 126:12184–12190.

Ude, S., Fernandez de la Mora, J., Alexander, J. N., and Saucy, D. A. (2006). Aerosol Size Standards in the Nanometer Size Range. II. Narrow Size Distributions of Polystyrene 3–11 nm in Diameter, *J. Colloid and Interface Sci*. 293:384–393.